

Supporting Information

Biomimetic Self-coacervation Adhesive with Tough Underwater Adhesion for Ultrafast Hemostasis and Infected Wound Healing

Tingwu Liu,^{a,b} Wen Sun,^{a,b} Xu Zhang,^a Donghua Xu,^a Mingzhe Wang,^a Qiuyan Yan,^{*,a} Jinghua Yin,^a and Shifang Luan,^{a,b}

^a *State Key Laboratory of Polymer Physics and Chemistry, Changchun Institute of Applied Chemistry, Chinese Academy of Sciences, Changchun 130022, P. R. China*

^b *University of Science and Technology of China, Anhui 230026, P. R. China*

* Corresponding author.

E-mail address: gyyan@ciac.ac.cn

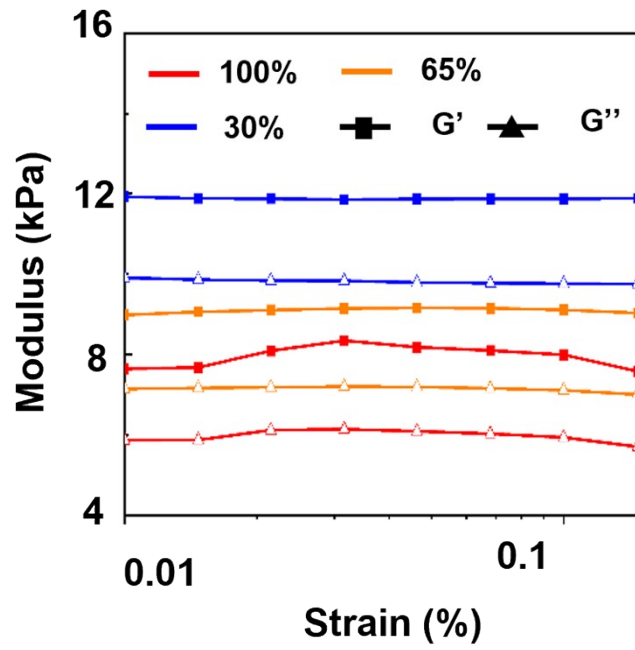


Figure S1. Storage modulus (G') and loss modulus (G'') of d-PGA/LZM with different hydration ratio.

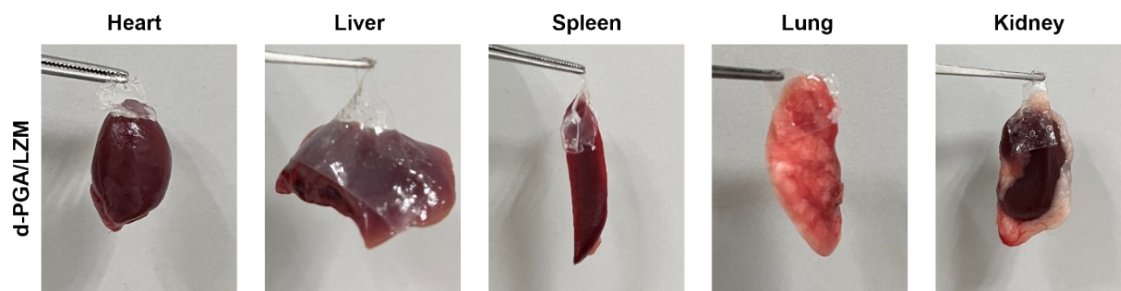


Figure S2. Wet adhesion properties of d-PGA/LZM in rat fresh organs or tissues.

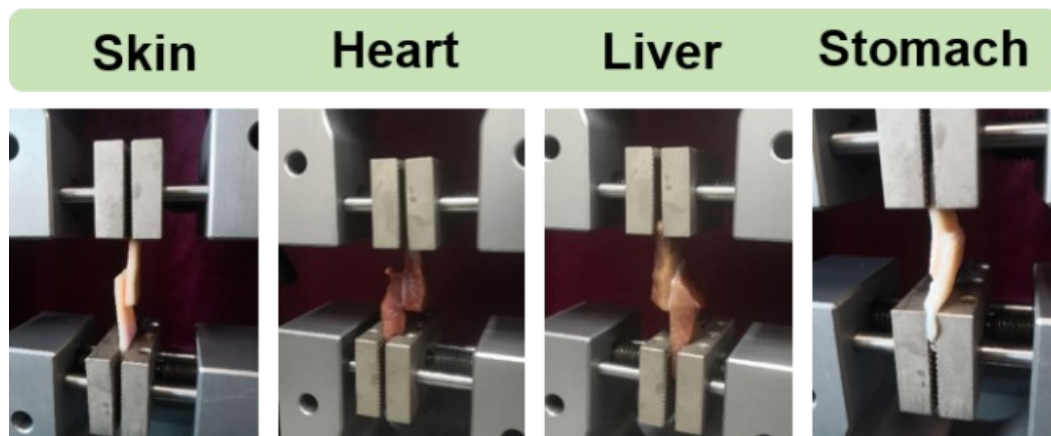


Figure S3. Photographs showing strong adhesions of the d-PGA/LZM adhesives with different soft tissue (porcine skin, heart, liver and stomach).

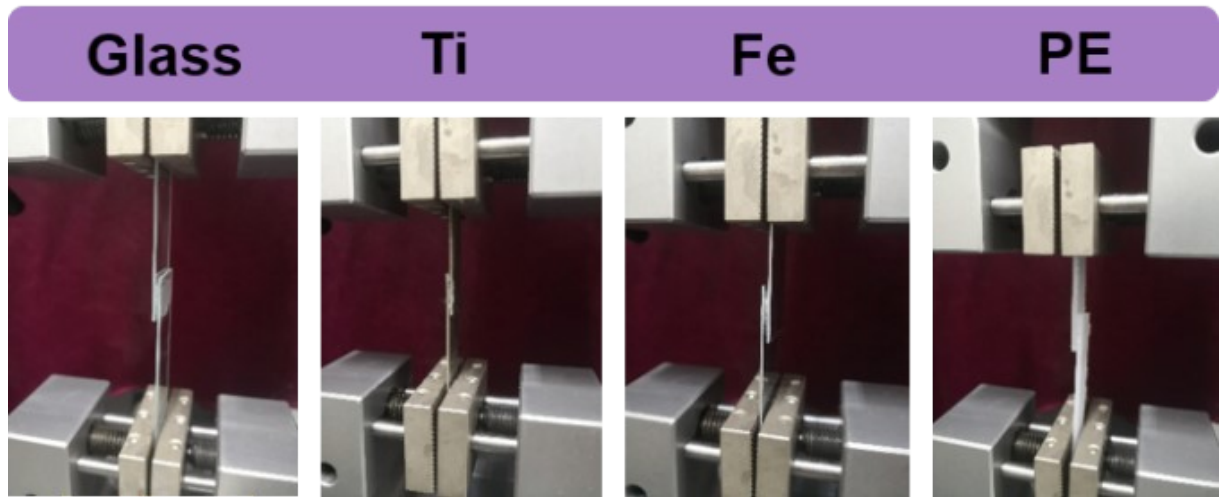


Figure S4. Photographs showing strong adhesions of the d-PGA/LZM adhesives with different hard substrate (Glass, Ti, Fe and PE).

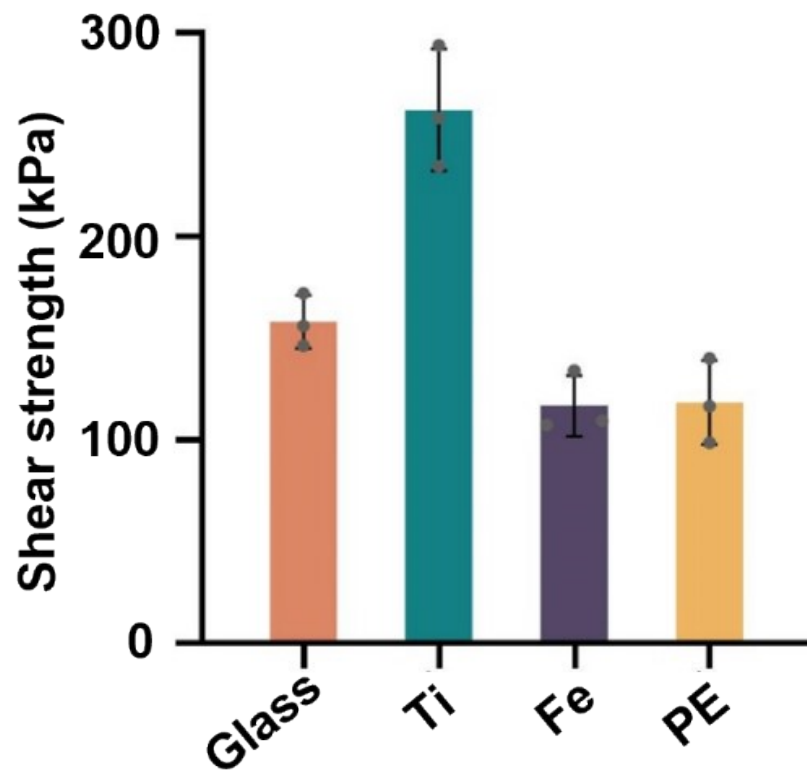


Figure S5. Adhesion strength of d-PGA/LZM adhesives on various substrate.

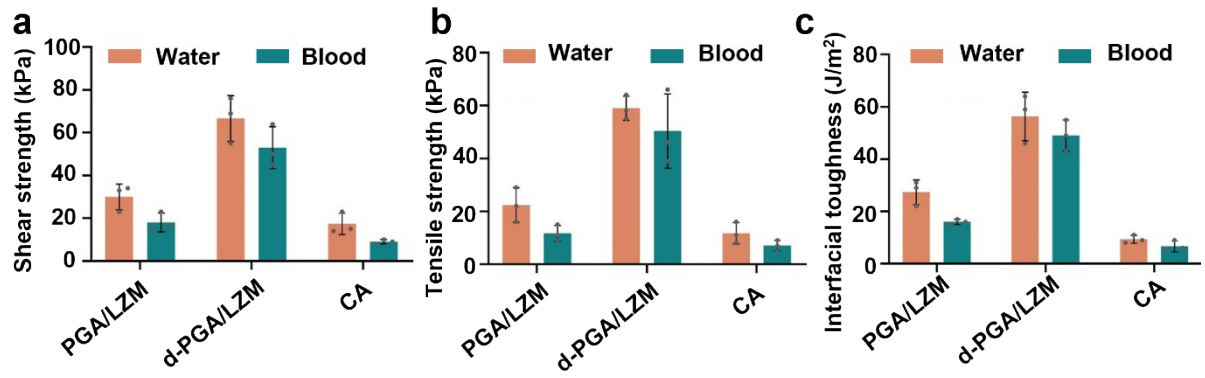


Figure S6. Lap-shear strength, tensile strength, and interfacial toughness of d-PGA/LZM on wet pig skin.



Figure S7. Strong and stable adhesion enable d-PGA/LZM to hold a 100 g weight immersed in

water for 7 days.

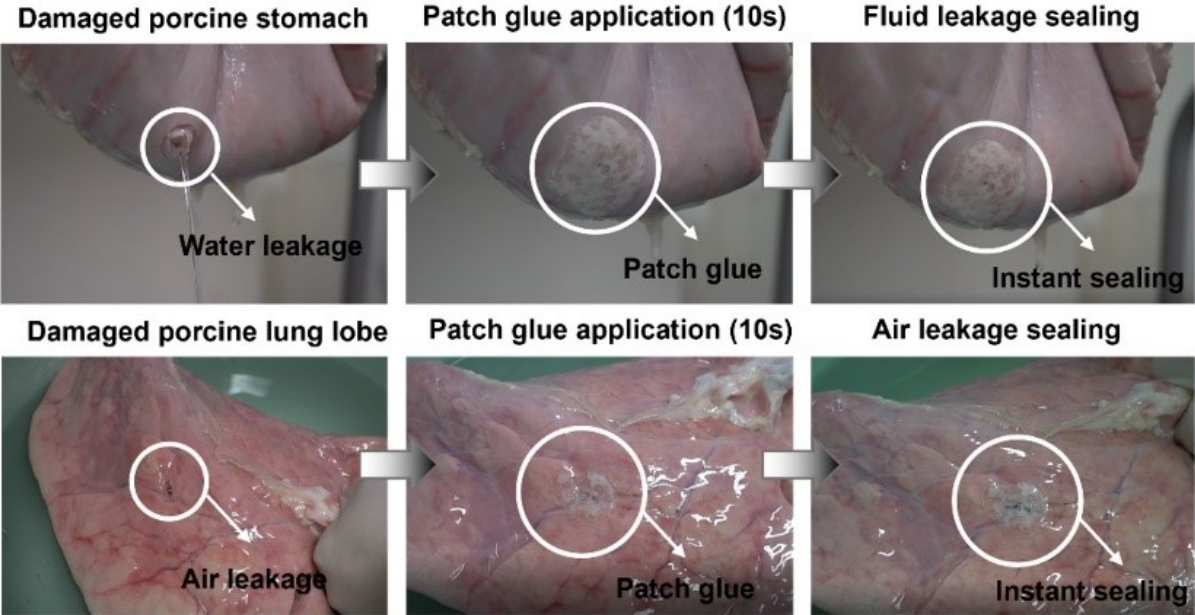


Figure S8. Sealing of a water-leaking porcine stomach and an air-leaking porcine lung using d-PGA/LZM adhesive.

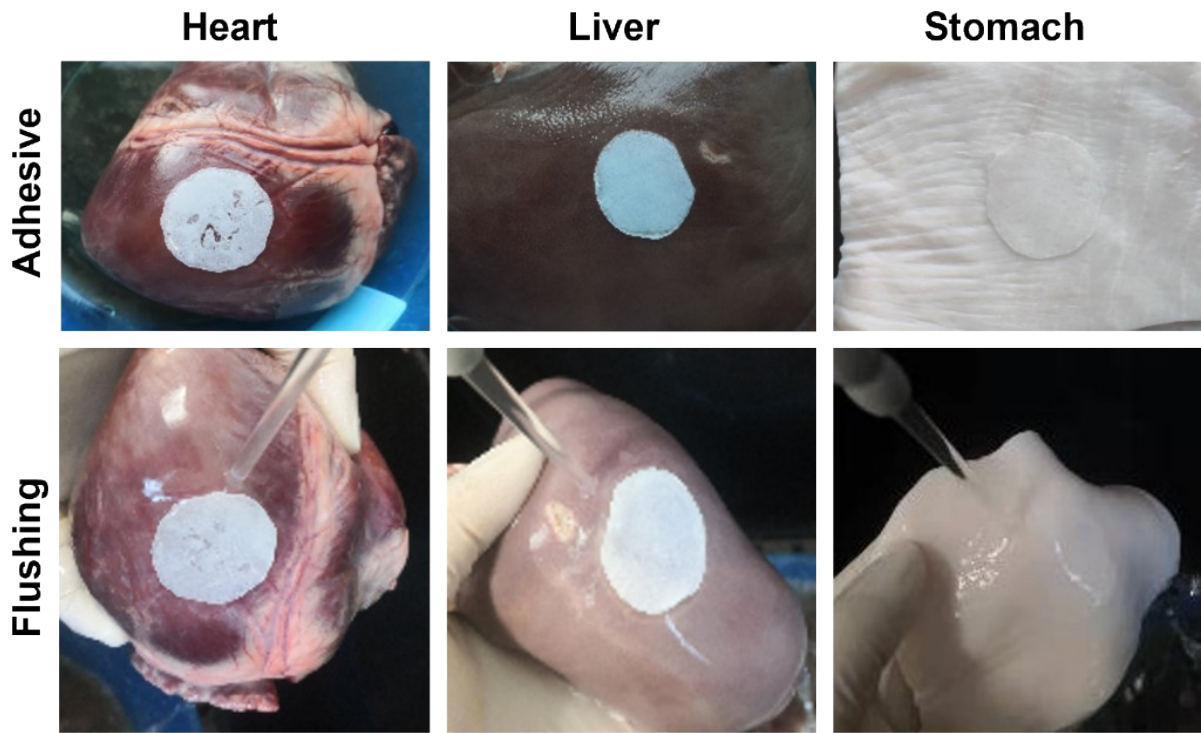


Figure S9. Porcine heart, liver and stomach adhered by d-PGA/LZM adhesive and withstand water impact.

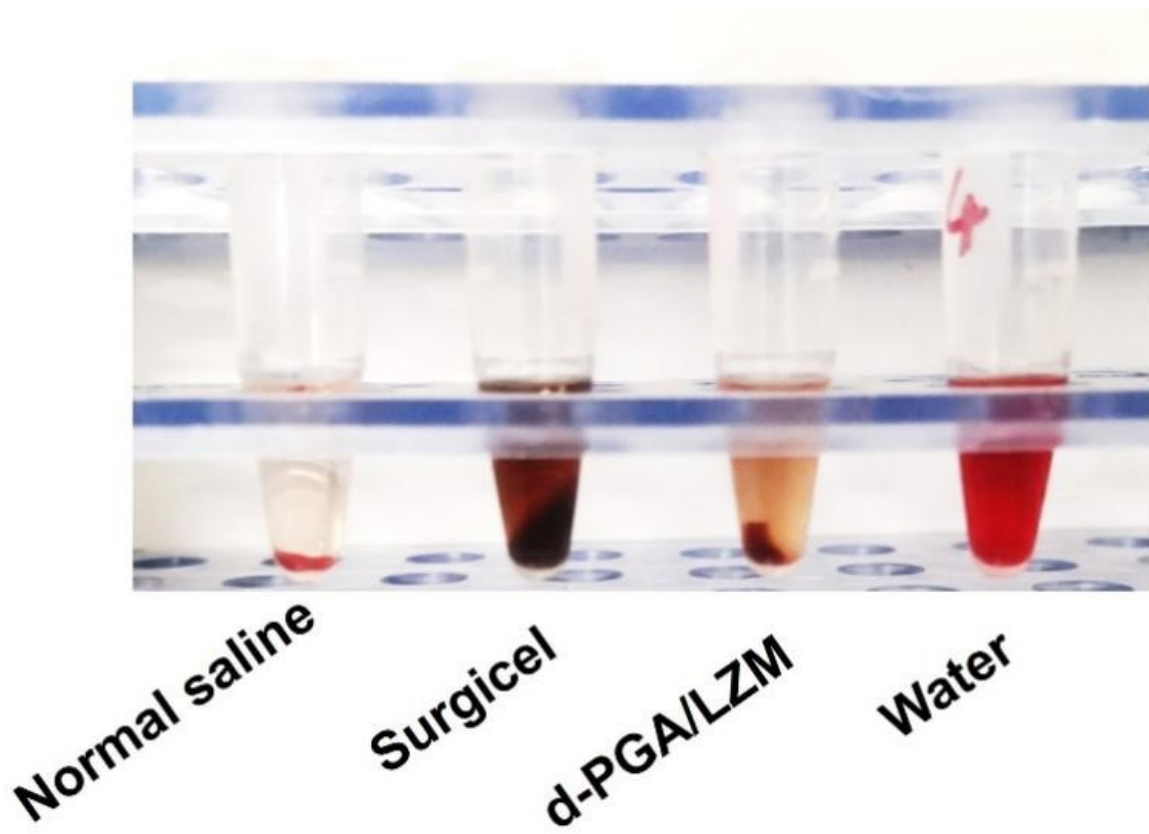


Figure S10. Optical images of hemocompatibility of surgical and d-PGA/LZM.

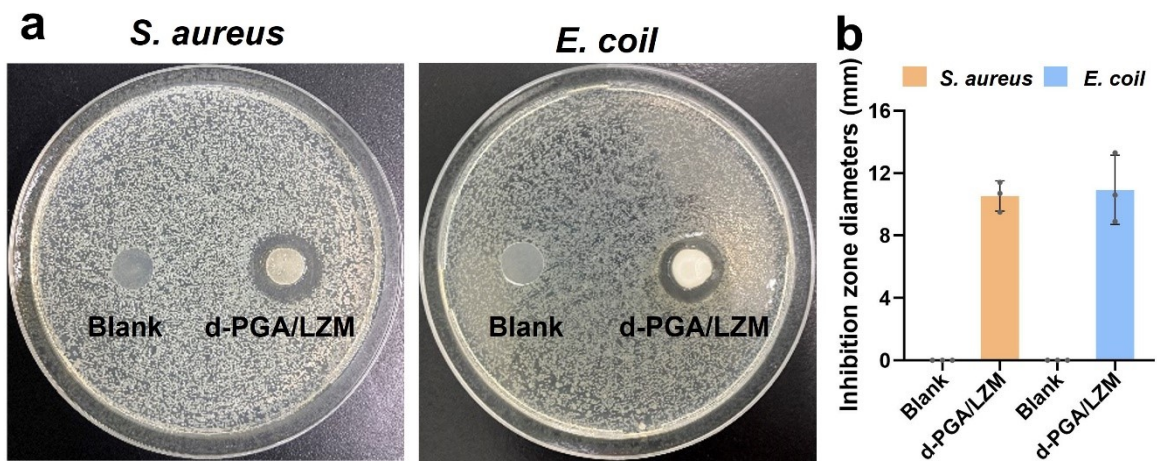


Figure S11. a) Zone of inhibition test for antimicrobial activity and b) quantitative antibacterial results of PE thin film and d-PGA/LZM against *E. coli* and *S. aureus*.

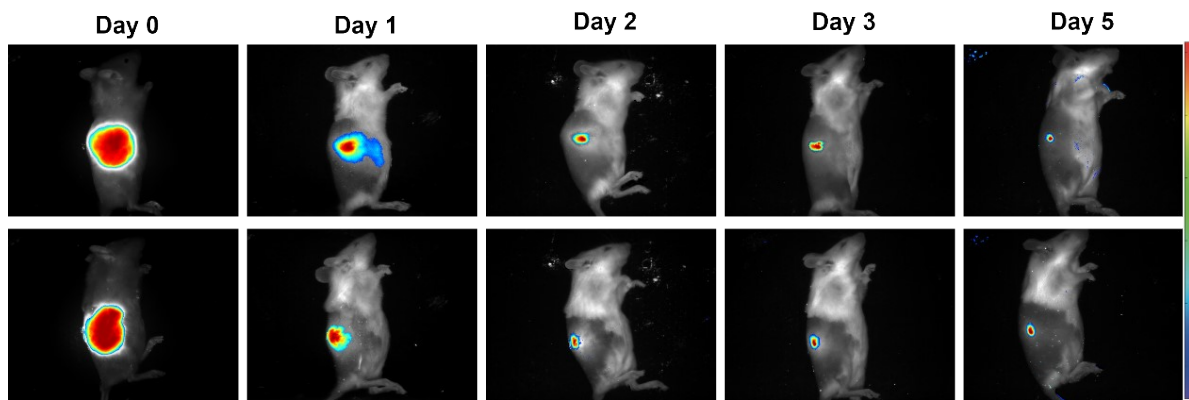


Figure S12. Pictures of the *in vivo* imaging showing the *in vivo* degradation of d-PGA/LZM labeled by FITC on the subcutaneous muscle.

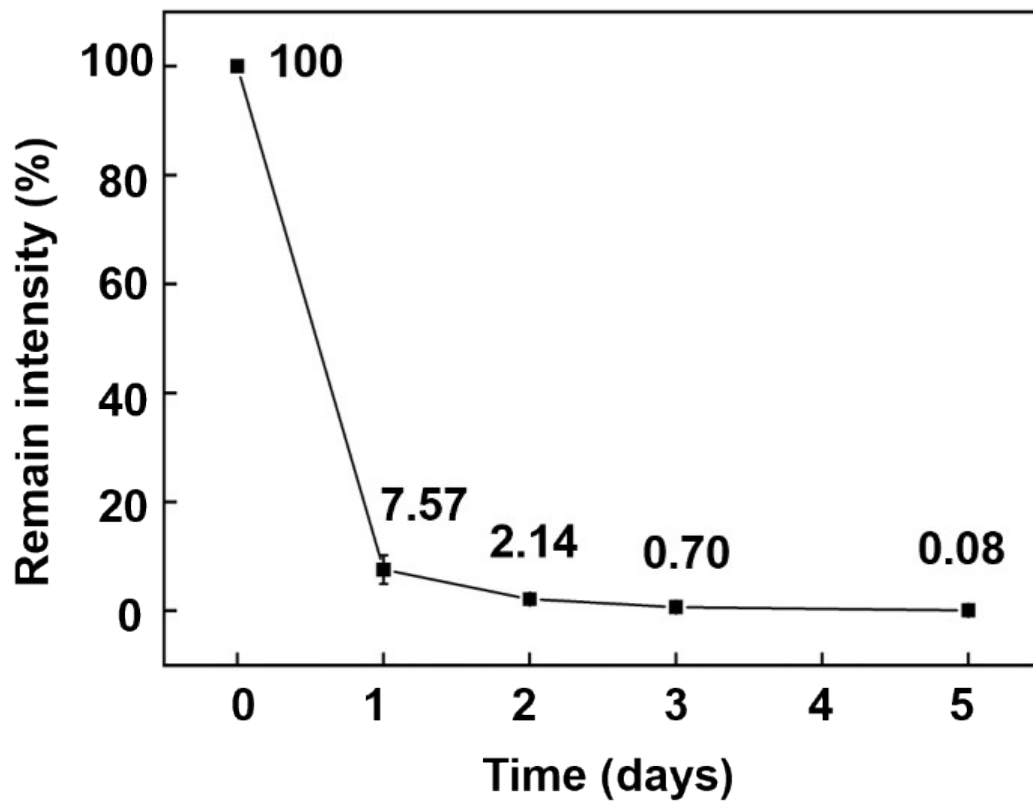
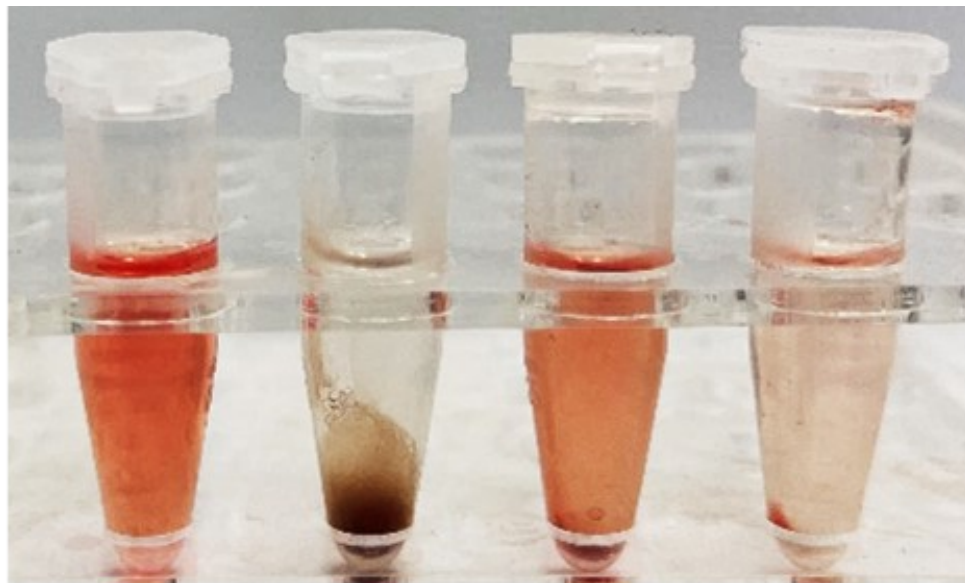


Figure S13. Time-dependent *in vivo* imaging showing the *in vivo* degradation of d-PGA/LZM adhesive labeled by FITC on the subcutaneous muscle.



Control
Surgicel
CA
d-PGA/LZM

Figure S14. Photographs of blood clotting at 150 s.

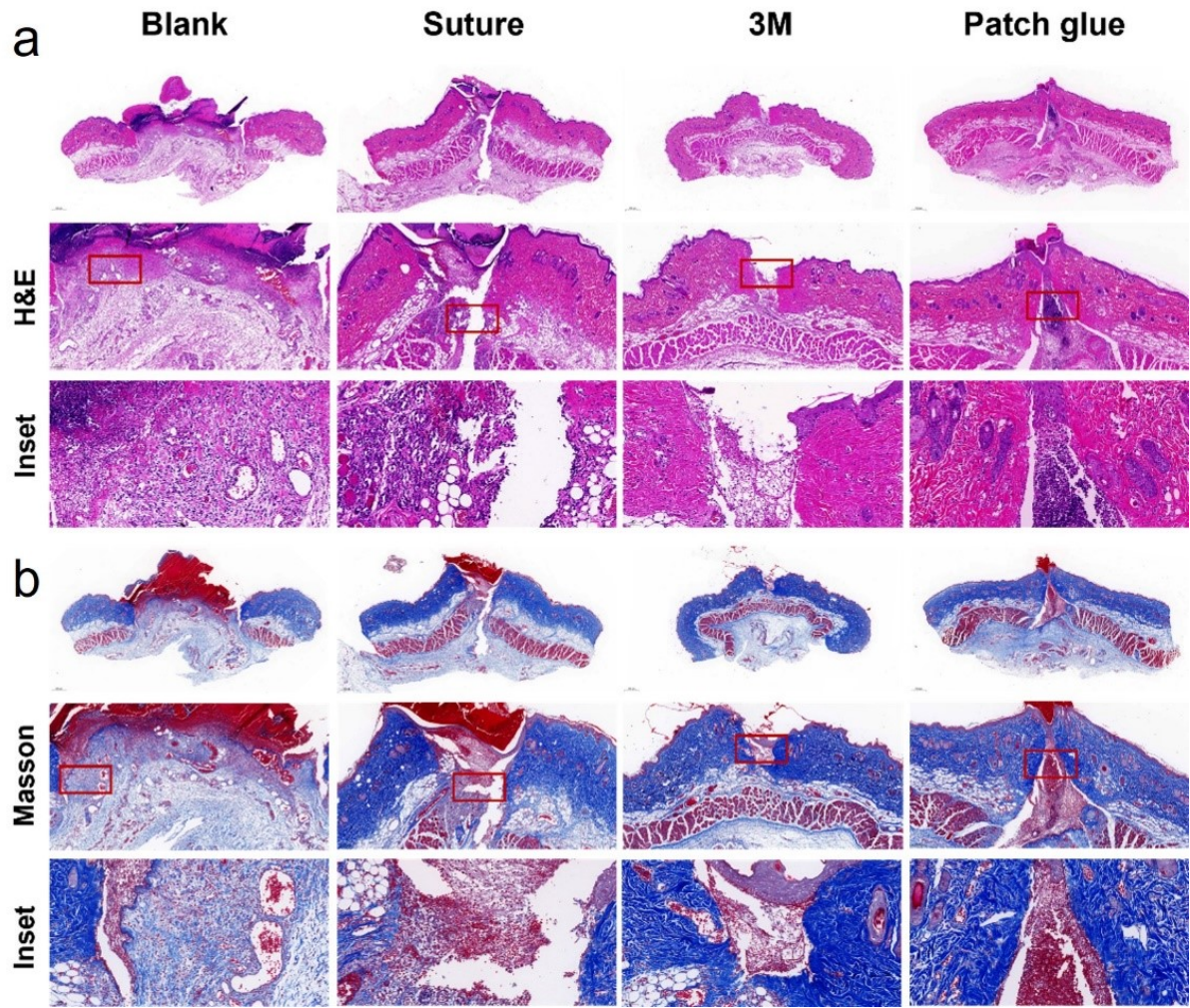


Figure S15. a, b) Histological analysis of the wounds stained with H&E (a) and Masson (b) on day 3.

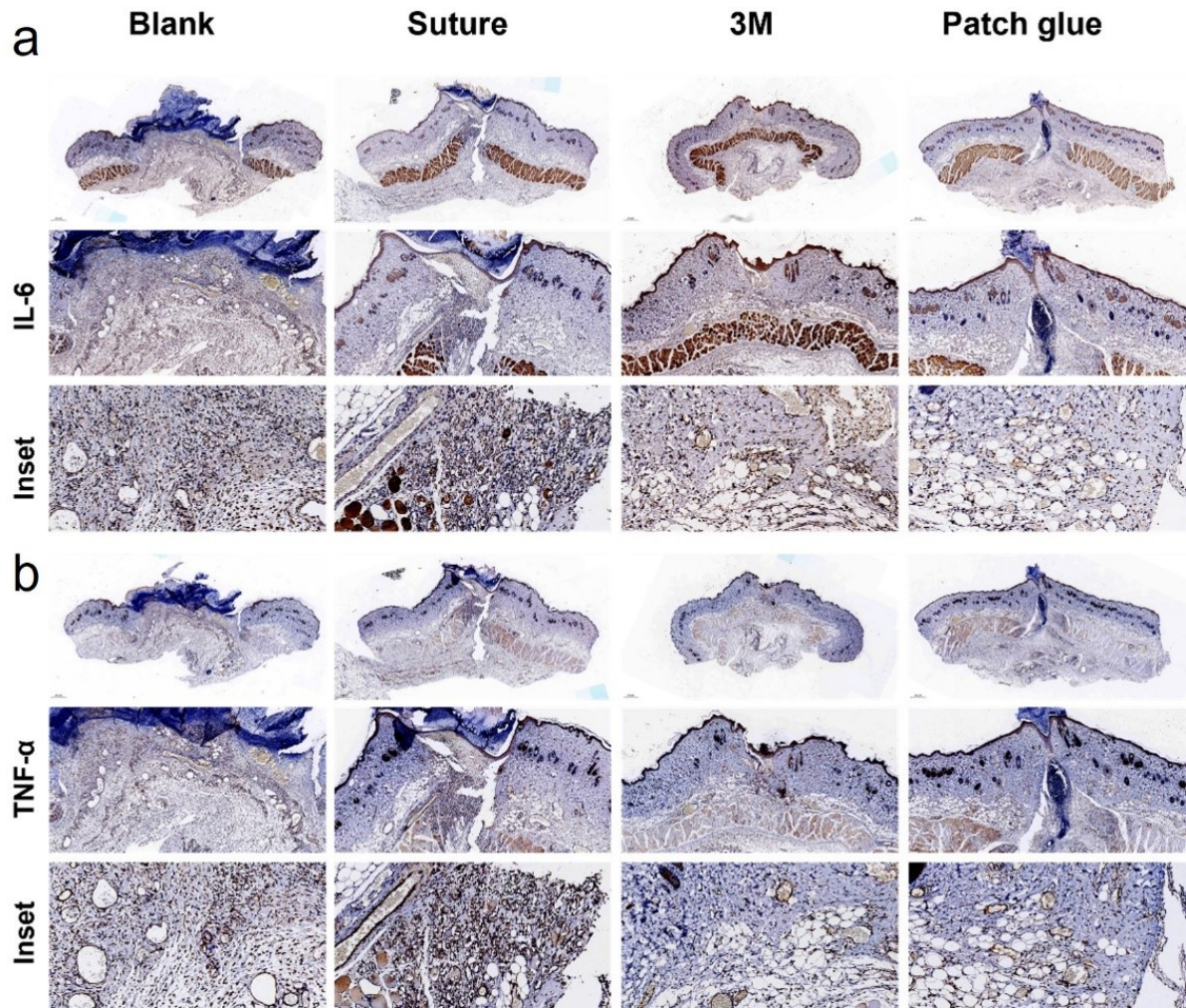


Figure S16. h, j) Immunohistochemical staining of IL-6 (h) and TNF- α (j) at wound sites on day 3. Yellow arrowheads indicate the positive TNF- α and IL-6 staining.

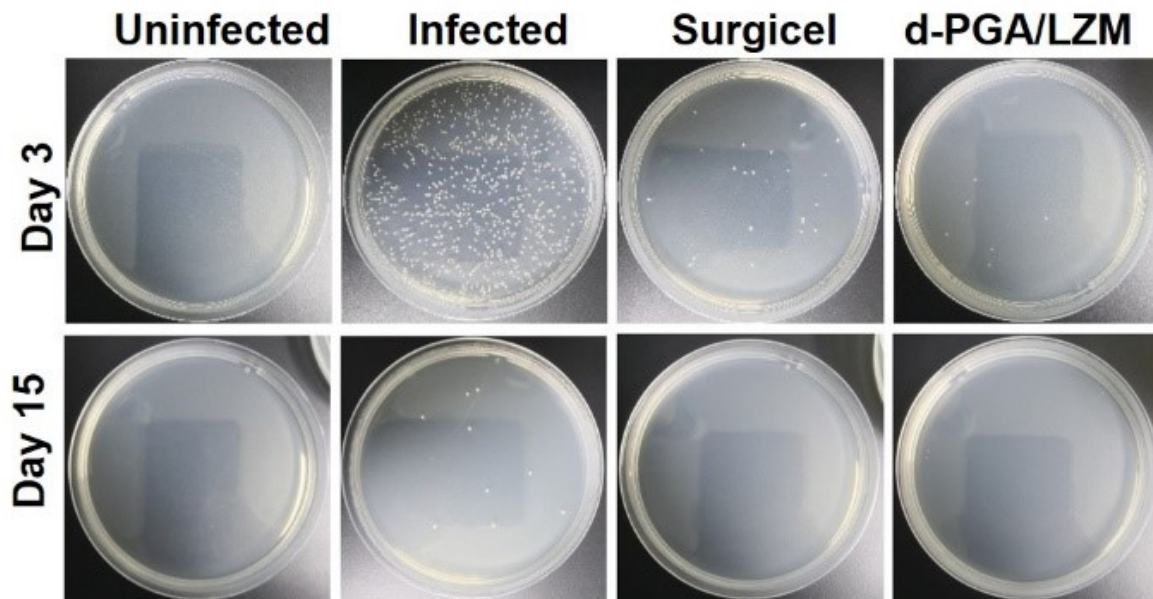


Figure S17. Photoscopic image of bacterial colony-forming units obtained from the wound tissues after day 3 and 15.

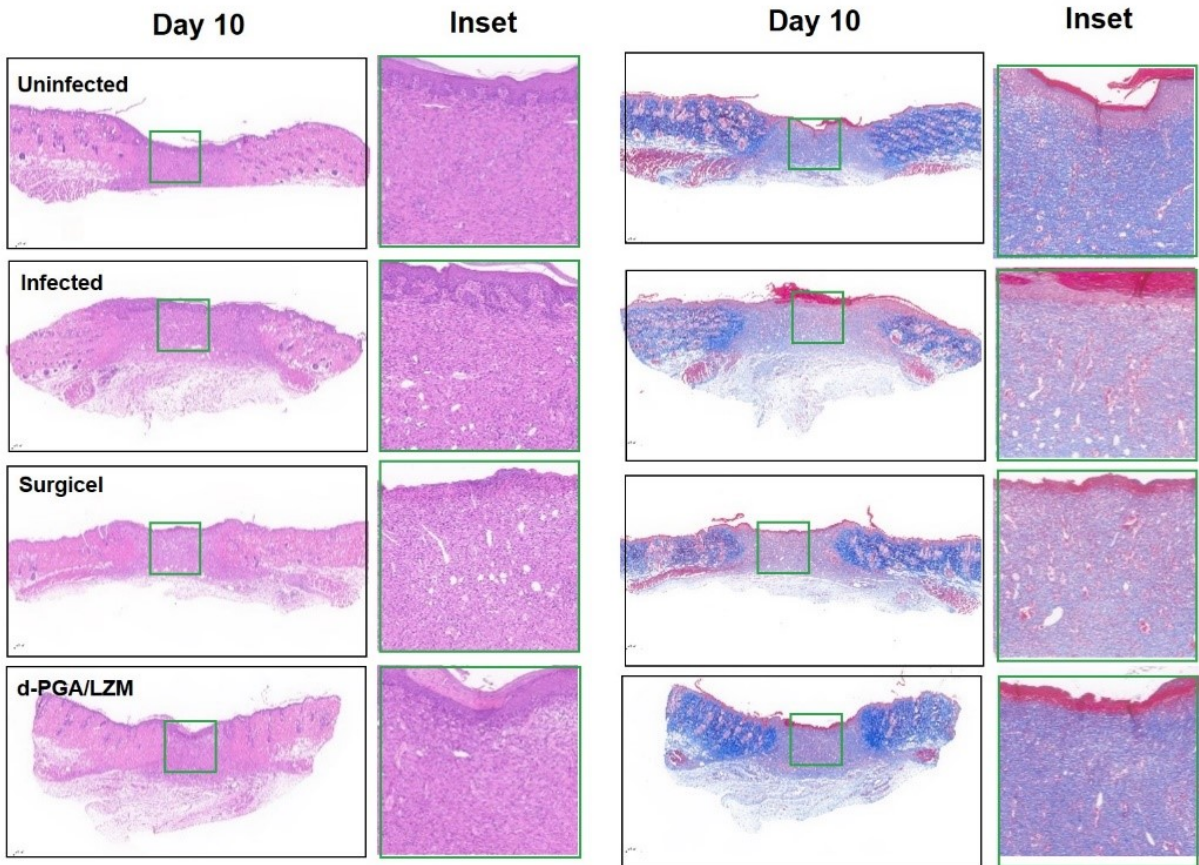


Figure S18. H&E-stained and Masson staining images of the wound tissue on day 10.